Impact of interfermionic forces on the pair-creation process

A. T. Steinacher, R. E. Wagner, Q. Su, and R. Grobe
Intense Laser Physics Theory Unit and Department of Physics, Illinois State University, Normal, Illinois 61790-4560, USA
(Received 17 December 2013; revised manuscript received 11 February 2014; published 17 March 2014)

Using a simplistic model in one spatial dimension, we estimate the impact of the electron-electron, positron-positron, and electron-positron forces on the yield of the pair-creation process triggered by an external superstrong force. We separate the scalar and vector potentials in the Dirac equation into external and internal parts, where the dynamics of the internal potentials are governed by the Maxwell equations with the Dirac charge and current densities as source terms. In order to explore the impact of the interfermionic forces, we compute the number of created pairs, the time evolution of the charge, and current density as well as the electronic and positronic spatial probability density. We find that once the particle pair is created, the electron-positron attraction keeps the particles from being accelerated out of the interaction zone and the resulting Pauli blocking suppresses the pair-creation process. On a longer time scale, however, the forces lead to an enhancement of pair creation.

DOI: 10.1103/PhysRevA.89.032119 PACS number(s): 12.20.−m, 03.65.−w, 34.50.Rk

I. INTRODUCTION

The prospect of producing an electron-positron pair from the vacuum triggered by a supercritical field has led to wide theoretical interest [1–6]. However, all studies have neglected the field theoretical Coulombic interactions between the created particles. On an accurate quantum field theoretical level, interfermionic interactions are facilitated by the second quantized photon field, which would have to be treated as an independent dynamical quantity with its own dynamics. Unfortunately, due to the present computational limitations and also many conceptual problems, such as renormalization and particle dressing, this approach is presently out of reach. A first valuable insight into the effect of the back reaction on the pair-creation process was provided by coupling the quantum kinetic Vlasov equation for the particles' momentum density to the Maxwell equations [7–11]. This approach provides remarkable insight and is ideally suited to study the prediction of nonequilibrium quantum mean-field theory for three-dimensional environments for spatially homogeneous fields. These works are similar to our work discussed below in the sense that they also separate between an external and a self-consistent internal field, whereas the recent work by Hebenstreit and colleagues [12,13] used a one-dimensional model system and studied a single and fully coupled initial field. These studies suggest that the back coupling might reduce the yield of the created particles. It is presently not known how these forces would affect the dynamics or by how much the famous Schwinger threshold field [14,15] for the pair creation can be increased or even decreased when these effects are taken into account for a spatially localized three-dimensional interaction. This question becomes even more urgent, as new laser-based experiments are being planned at various laboratories [16].

In order to get a very rough order of magnitude estimate, one could assume for a moment that the usual nonrelativistic Coulomb law was valid even on the smallest spatial scales relevant for the pair-creation process. This length scale is certainly much shorter than the electron's Compton wavelength, $\lambda = h/(mc)$ ($\approx 2.4 \times 10^{-12}$ m), which is the wavelength of a photon that has an energy equal to the electron's rest energy, mc^2 ($\approx 8.2 \times 10^{-14}$ J). The Coulomb energy between an electron and positron at this distance from each other is kq^2/λ ($\approx 9.5 \times 10^{-17}$ J), which would be about 860 times smaller than the electron's rest energy. So if the electron-positron pair's separation during its creation were actually larger than the Compton wavelength and *if* the classical Coulomb force law was valid in this form, one could tentatively neglect interfermionic forces. However, the validity of both of these assumptions is presently not established. A recent quantum field theoretical model calculation [17] has suggested that even the direction of the force between two charges can depend on which modes of the second-quantized photon field are permitted.

The purpose of this work is twofold. First, we try to examine the computational feasibility for a possible theoretical framework to include (still on an approximate level) the three interfermionic forces. Here the pair creation is governed by the Dirac equation and the internal field is approximated by a classical elecromagnetic field whose space-time evolution is determined by the Maxwell equations. To study the feasibility of such an approach we used a one-dimensional system. This has the advantage that, in addition to computational challenges, conceptual problems concerning the directions of the forces can also be addressed. The second goal is to use the data produced by this model to obtain some qualitative insight into the pair-creation dynamics and therefore give direction to for further study.

The paper is organized as follows. In Sec. II we introduce the coupled Dirac-Maxwell equations for our one-dimensional model system. In Sec. III we show that a "single-particle" Dirac wave function is able to predict the mutual repulsion between electrons (and similarly for positrons) and at the same time the attractive force between electronic and positronic portions of the same wave function. Being able to obtain the expected direction of the three interfermionic forces within a single wave function is an important consistency test for the proposed formalism. In Sec. IV we compare the pair-creation dynamics with and without internal interactions among the created particles. In Sec. V we provide a discussion of possible open questions that will be addressed in future work.

II. ONE-DIMENSIONAL MODEL SYSTEM

A. Electron-positron dynamics

We model the pair-creation process of electron-positron pairs by the time-dependent Dirac Hamiltonian in one spatial dimension [18],

$$h(q) = c\sigma_1[p - q/cA(z,t) - q/cA_{\rm ext}(z)] + \sigma_3 mc^2 + qV(z,t) + qV_{\rm ext}(z), \tag{2.1}$$

where c is the speed of light and σ_1 and σ_3 are the two Pauli matrices. In our numerical simulations below we use atomic and cgs units, where the four fundamental constants [amount of the charge of the electron $|q|$, its mass m, and Coulomb's and Planck's constants $1/(4\pi\varepsilon_0)$ and $\hbar$] are all unity by definition. As a result, the speed of light is $c = 137.036$ a.u. For $q = -1$ [$q = 1$], the Hamiltonian $h(e^-)$ [$h(e^+)$] describes the evolution of an electron [positron]. As the external potentials act only along the z direction and do not mix spin components, $h(q)$ can govern the time evolution of the nonvanishing spinor components. Equation (2.1) can be easily derived from the usual three-dimensional Dirac Hamiltonian for the four-spinor component wave functions, $c\,\boldsymbol{\alpha}\,\mathbf{p} + mc^2\beta$, with the usual 4×4 matrices $\boldsymbol{\alpha} = (\alpha_x,\alpha_y,\alpha_z)$ and β. The energy eigenstates with positive energy $w_p \equiv [m^2c^4 + c^2p^2]^{1/2}$ are proportional to $[\mathbf{s}, c\boldsymbol{\sigma}\mathbf{p}\mathbf{s}/(mc^2 + w_p)]$, where $\mathbf{s}$ is a two-component vector. When we assume $\mathbf{s} = (1,0)$ and $p_x = p_y = 0$ we can eliminate the vanishing second and fourth spinor component from our notation and obtain Eq. (2.1).

The energy eigenstates of the force-free Hamiltonian (denoted by h_0) with momentum p in the positive (up) energy continuum are denoted by $h_0|u;p\rangle = w_p|u;p\rangle$ whereas those in the negative ($d$own) continuum are denoted by $h_0|d;p\rangle = -w_p|d;p\rangle$. In the literature they are also wisely called positon and negaton states [19]. Their spatial representation is given by

$$\langle z|u;p\rangle \equiv W_p(u;z) = \chi[1, cp/(mc^2 + w_p)]\exp[ipz], \tag{2.2a}$$

$$\langle z|d;p\rangle \equiv W_p(d;z) = \chi[-cp/(mc^2 + w_p), 1]\exp[ipz], \tag{2.2b}$$

where $\chi \equiv (2\pi)^{-1/2}[1 + c^2p^2/(w_p + mc^2)^2]^{-1/2}$ denotes the normalization factor. While both states have the same momentum eigenvalue p, the state in Eq. (2.2b) would evolve in the direction opposite of p under h_0. Furthermore, if the Hamiltonian has nonvanishing external potentials as in Eq. (2.1), then a superposition of the states $W_p(u;z)$ would be accelerated in the opposite direction than states consisting of $W_p(d;z)$. As it will be important for our discussion below, we note here that the antilinear operator $C \equiv \sigma_1 K$ (where K denotes complex conjugation) can convert a positive energy state with momentum p into a state with negative energy and reversed momentum, $\sigma_1 K|u;p\rangle = |d,-p\rangle$.

While in any description the (up) states $|u;p\rangle$ are usually associated with electrons, the interpretation of the mathematical (down) states $|d;p\rangle$ depends on the theory. As we will discuss below, in relativistic quantum mechanics their charge conjugated form is viewed as positron states, whereas in Dirac's quantum field theory their occupation represents the vacuum.

The two interaction terms in h, $-\sigma_1 qA + qV$, generate the time evolution of a state associated with an electron if we choose a negative charge $q = -1$. In order to propagate the state for a positron, in principle one could choose the Hamiltonian of Eq. (2.1), but with a positive charge $q = 1$, which we have denoted by $h(e^+)$. However, using a different form of the Hamiltonian for each type of charge is not advantageous for dynamics that contain multiple particles and require a uniform description. Fortunately, the two Hamiltonians $h(e^-)$ and $h(e^+)$ can be related to each other via the (antilinear) charge-conjugation operator, $h(e^+) = -Ch(e^-)C^{-1}$, which effectively reverses the sign of the scalar and vector potentials in h. Here $C = \sigma_1 K$ can be represented as the product of σ_1 and the complex-conjugation operator K, where $KpK = -p, \sigma_1\sigma_1\sigma_1 = \sigma_1$ and $\sigma_1\sigma_3\sigma_1 = -\sigma_3$. The time evolution of an electronic state follows from $i\hbar\partial_t|e^-(t)\rangle = h(e^-)|e^-(t)\rangle$ and we will discuss in Sec. III A that it can be used to predict simultaneously also the corresponding solution of a positron, whose time evolution is normally governed by $i\hbar\partial_t|e^+(t)\rangle = h(e^+)|e^+(t)\rangle$. These considerations are important below, where we will show that a "single-particle" wave function can simultaneously describe a state with an electronic as well as positronic portion.

The vector and scalar potentials $A_{\rm ext}(z,t)$ and $V_{\rm ext}(z,t)$ in Eq. (2.1) represent a superstrong external field that can trigger the pair-creation process from the vacuum. The internal potentials $A(z,t)$ and $V(z,t)$ represent the fields that are generated by the particles and facilitate their mutual interaction. Their dynamical evolution is governed by the Maxwell equations described in the next section.

B. Dynamics of the internal fields $A(z,t)$ and $V(z,t)$

The Maxwell equations $\partial_t E = -4\pi\partial_t P$ and $\boldsymbol{\nabla}\cdot E = -4\pi\boldsymbol{\nabla}\cdot P$ determine the electric field from the polarization P (where $Q = -\boldsymbol{\nabla}\cdot P$) and simplify significantly due to the spatial limitation to only one dimension [20] to $\partial_z E = 4\pi Q$ and $\partial_t E = -4\pi J$, where $Q(z,t)$ and $J(z,t)$ are the charge and current densities, obtained from the Dirac wave function and fulfilling the required continuity equation $\partial_t Q + \partial_z J = 0$. In Appendix A we summarize the more general formalism of quantum electrodynamics in one spatial dimension.

Due to this spatial limitation, there is no magnetic field and the electric field E outside a charge distribution does not depend on the position. For example, according to Gauss's law, the static electric field associated with a localized negative unit charge at $z = -d$ and a positive one at $z = d$, i.e., $Q(z) = -\delta(z + d) + \delta(z - d)$, is simply given by the product of two Heaviside unit step functions, $E(z) = -4\pi\theta(z + d)\theta(d - z)$, corresponding to a constant field $E = -4\pi$ inside the dipole and $E = 0$ outside, where we have arbitrarily chosen $E(-\infty) = 0$. Also, the electric field associated with a localized positive unit charge [$Q(z) = \delta(z)$] is $E(z) = -2\pi + 4\pi\theta(z)$. As a result the corresponding electric potential difference between locations $z = 0$ and $z > 2c^2/(4\pi)$ exceeds $2c^2$ and is therefore automatically supercritical.

If we introduce the potentials V and A such that $E = -\partial_z V - \partial_{ct} A$, the two Maxwell equations read $\partial_z \partial_{ct} A + \partial_z^2 V = -4\pi Q$ and $c\partial_{ct}^2 A + c\partial_z \partial_{ct} V = 4\pi J$. Using the Lorenz [21,22] gauge, $\partial_z A = -c^{-1}\partial_t V$, we obtain the two separate equations for the potentials,

$$\left(\partial_{ct}^2 - \partial_z^2\right) V = 4\pi Q(z,t), \tag{2.3a}$$

$$\left(\partial_{ct}^2 - \partial_z^2\right) A = 4\pi c^{-1} J(z,t). \tag{2.3b}$$

Special attention has to be paid to the boundary conditions for our numerical box of total length L. As the Dirac equation for the wave function $\phi(z)$ can be solved most efficiently with periodic boundaries, $\phi(-L/2) = \phi(L/2)$, we choose them also for the electric potentials. However, there is an unavoidable consequence due to this choice. Gauss's law prohibits that the electric field associated with a periodic charge can be periodic as well, in other words, we have $E(-L/2) \neq E(L/2)$. This discontinuity acts numerically like an additional unphysical charge at $z = \pm L/2$, to which any portion of the Dirac wave function that is located there would react.

Furthermore, the required periodicity $V(-L/2) = V(L/2)$ leads to an unphysical box-size-dependent electric field if L is finite. For example, the (periodic) potential associated with a positive unit charge located at $z = a$ (>0), $Q(z) = \delta(z - a)$ is given by $V(z) = -4\pi[\theta(z-a)(z-a) + z(a/L - 1/2)]$, which leads to the electric field $E(z) = 4\pi[\theta(z-a) + (a/L - 1/2)]$. Here $\theta(x) = x/|x|$ denotes again the Heaviside unit step function. As a result, a positive test unit charge placed at $z = 0$ would experience the repulsive L-dependent force $E(0) = -4\pi(1/2 - a/L)]$. This unavoidable L-dependent force can be also visualized as the periodic boundaries constrain the fields and particles to a ring of effective diameter L. While the probe at $z = 0$ is repelled by the charge at $z = a$ to the left, due to the ring geometry the same charge is also located at distance $L-a$ to the left of it and would therefore push it to the right.

In fact, if the first charge is not placed at $z = a$ but at $z = L/2$, the two resulting oppositely directed forces on the test charge at $z = 0$ would cancel completely, $E(0) = 0$, in this case. As we will show below, due to causality (finite propagation speed of any field) these undesirable numerical features (due to a finite L) fortunately do not compromise the solutions to the Maxwell-Dirac equations. These features only limit the maximum interaction time of our simulations.

In order to have comparable magnitudes for the one- and three-dimensional forces, we can introduce a unitless scaling factor κ in front of the charge and current density in the Maxwell equations. For example, the three-dimensional (3D) Coloumb electric field due to a unit charge at a distance given by the electron's Compton wave length $(\lambda = 1/c)$ is $E_{3D} = 1/r^2 = c^2$, while the corresponding 1D field is $E_{1D} = 2\pi$. If we use a factor $\kappa = c^2/2\pi$ the two forces would be identical at the distance λ. In our numerical calculations below we use various prefactors before the internal potentials in the Dirac equation and the charge and current densities in the Maxwell equations. In order to solve the coupled Maxwell-Dirac equations, we have used FFT-based split-operator technique [23–27] for the Dirac equation and a finite-difference based and also FFT-based algorithm to solve the Maxwell equations. The algorithmic details are presented in Appendices B and C.

III. INTERNAL DYNAMICS FOR NO EXTERNAL FIELDS, $A_{ext} = V_{ext} = 0$

We examine using the fully coupled Dirac-Maxwell equation to study pair creation in a dynamical context with full space-time resolution. While there are some early works [28–39] that have examined the mathematical properties and stability of various numerical algorithms for these equations for a single charge, it is necessary to confirm first if our formalism can actually produce reasonable predictions for the time evolution of the particles in the absence of any external field.

A. Single-particle dynamics of an electron or positron

Due to their opposite charges, electrons and positrons are differently coupled to external and internal fields, as described by $h(e^-)$ and $h(e^+)$. However, due to a symmetry relationship between $h(e^-)$ and $h(e^+)$ under charge conjugation, the same Hamiltonian $h(e^-)$ can be used to describe the time evolution of both types of particles. The initial state for an electron $|e^-(t=0)\rangle$ is always chosen as a superposition of states $|u;p\rangle$ with positive energy [see Eq. (2.2a)]. As the Hamiltonians h_0 for electrons and positrons are identical in the absence of any potential, also the initial positronic state has to be a superposition of *positive* energy states, $|e^+(t=0)\rangle = \Sigma_p \alpha_p |u;p\rangle$ with expansion coefficients α_p.

In the presence of internal and external potentials, the time evolution of the electronic state is governed by $h(e^-)$, leading to $|e^-(t)\rangle = U(e^-)\,|e^-(t=0)\rangle$. In the propagator $U(e^-) \equiv T\exp[-i\int^t d\tau\, h(e^-)]$, T is the required time-ordering operator as the potentials A and V are generally time dependent. On the other hand, the time evolution for the state of the positron $|e^+\rangle$ would be governed by a different Hamiltonian $h(e^+)$, leading to $|e^+(t)\rangle = U(e^+)\,|e^+(t=0)\rangle$, where the corresponding propagator is naturally given by $U(e^+) \equiv T\exp[-i\int^t d\tau h(e^+)]$.

It turns out, however, that we can also use the "electronic" propogator $U(e^-)$ to obtain the time evolution of the positron state $|e^+(t)\rangle$ using a "detour" based on the charge-conjugation operator C introduced in Sec. II A. Applying $U(e^+) = CU(e^-)C$ to the solution $|e^+(t)\rangle = U(e^+)\,|e^+(t=0)\rangle$, we obtain $|e^+(t)\rangle = CU(e^-)C|e^+(t=0)\rangle = CU(e^-)\Sigma_p \alpha_p^* |d;-p\rangle \equiv C|s(t)\rangle$, where we have used that $C|u;p\rangle = |d;-p\rangle$. In other words, we can obtain the correct time evolution of the positronic state $\Sigma_p\,\alpha_p|u;p\rangle$, if we use the coefficients α_p and construct a "mirror" state as a superposition of negative energy states, $|s(t=0)\rangle = \Sigma_p \alpha_p^* |d;-p\rangle$ and use $U(e^-)$ to evolve this state in time leading to $|s(t)\rangle$. We can then use $|s(t)\rangle$ to obtain the resulting time evolved positron state $|e^+(t)\rangle$ at any instant of time by simply applying the charge conjugation to this mathematical state, $C|s(t)\rangle = |e^+(t)\rangle$. This means we have shown that we can use the same Hamiltonian $h(e^-)$ to compute the time evolution of electrons and positrons in the presence of external fields. In other words, we can describe the electron-positron (two-particle) state by a *single* wave

function for fields that are weak enough not to couple upper and lower continuum states. In case the fields are supercritical and these transitions become non-negligible, a true quantum field theoretical framework would be needed to correctly interpret the meaning of the data, similarly as shown in Ref. [40].

In order to model an initially spatially localized electron or positron that is initially centered at $z = 0$ and has a spatial width of Δz_0, we use the following two (identically chosen) initial states:

$$\langle z|e^-(t=0)\rangle = \left(2\Delta z_0^2/\pi\right)^{1/4} \int dp \exp\left[-p^2\Delta z_0^2\right] W_p(u;z)$$

for the electron, (3.1a)

$$\langle z|e^+(t=0)\rangle = C\left(2\Delta z_0^2/\pi\right)^{1/4} \int dp \exp\left[-p^2\Delta z_0^2\right] W_{-p}(u;z)$$

for the positron. (3.1b)

While a single electron or positron modeled by a quantum-mechanical wave function should not be able to interact with itself, the present description permits such an "unphysical" interaction due to the intrinsic statistical meaning of a wave packet. While according to the Born interpretation the spatial probability density represents only a temporal average of infinitely many measurements of the same single particle, in our approach (where the Maxwell field was not second-quantized) the whole spatial density acts as a source term in Maxwell equations, which then produces a field to react which all portions of the wave function simultaneously. In other words, different portions of the same particle wave packet can interact with themselves like particles in a classical ensemble of many particles or in a charge cloud.

In order to obtain the correct signs for the potentials V and A in a consistent manner from the Maxwell equation, we have used in this study the source terms $Q \equiv -\langle z|e^-(t)\rangle^\dagger \langle z|e^-(t)\rangle$ and $J \equiv -c\langle z|e^-(t)\rangle^\dagger \sigma_1 \langle z|e^-(t)\rangle$ for the simulation of the dynamics of the electron, while $Q \equiv \langle z|e^+(t)\rangle^\dagger \langle z|e^+(t)\rangle$ and $J \equiv c\langle z|e^+(t)\rangle^\dagger \sigma_1 \langle z|e^-(t)\rangle$ is used for the positron. We note that the charge-conjugation operator does not affect the corresponding charge or current density as ${\sigma_1}^2 = 1$.

In Fig. 1 we illustrate the unphysical self-repulsion for an electron wave packet. In addition to the final probability density $\langle z|e^-(t)\rangle^\dagger \langle z|e^-(t)\rangle$ we have also graphed by the dashed line the corresponding density in the absence of any interaction ($\kappa = 0$) for comparison, reflecting simply the usual quantum-mechanical spreading associated with the nonvanishing variance in momentum.

While the usual quantum wave packet spreading sets in only after a short time delay that is proportional to $1/\Delta z_0$ (as fast and slower portions of the packet are spatially equally distributed and need some time to evolve to the wings of the packet), the self-interaction sets in almost instantaneously. The same repelling self-interaction is also obtained for the positron, based on the initial state of Eq. (3.1b).

B. Time evolution of an electron-positron state

The Dirac equation is quite remarkable. While h is the fundamental generator of the time evolution in quantum field theory for the electron-positron field operator, it is

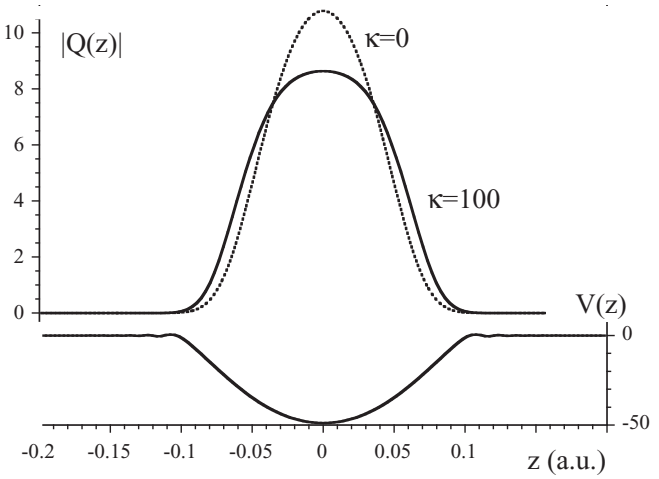

FIG. 1. The probability density of an electron wave packet $|Q(z,t)|$ with (solid line) and without (dashed line) the interaction potential $V(z,t)$ at final time $t = 0.1/c$. The corresponding potential (at time $t = 0$) which causes the self-interaction is shown below the probability distributions. (Parameters are $L = 0.4$ a.u., $N_z = 128$ spatial gridpoints, initial width $\Delta z_0 = 0.01$ a.u.)

sometimes also used for relativistic quantum mechanics [15]. If excitations to the negative energy continuum can be neglected, it can be interpreted as a single-particle equation or even as a relativistic generalization of the Schrödinger equation. However, in those dynamical regimes where the states of positive and negative energies are not coupled directly (no transitions between these two continua), we can use these two energy subsets to describe simultaneously an electron and a positron via a *single* wave function. Even more, if the internal vector potential satisfies the Maxwell equations with the corresponding fermionic charge and current density as sources, the "single-particle" wave function with its sole dependence on z and t can even describe the repulsive and attractive interaction forces (e^-–e^-, e^+–e^+ and e^-–e^+) appropriately.

We will now show that the resulting forces between an electron and a positron is attractive. We have prepared our initial state as linear superposition of a Gaussian wave packet that is solely composed of positive energy states and centered at location z_0 and the charged conjugated version of the *same state*, except that it is centered at $z = -z_0$,

$$|\Phi(t=0)\rangle = \int dp A(p) \exp[-ipz_0]|u;p\rangle + \int dp A(p) \exp[ipz_0]|d;-p\rangle, \quad (3.2)$$

where $A(p) \equiv 2^{-1/2}\left(2\Delta z_0^2/\pi\right)^{1/4}\exp[-p^2\Delta z_0^2]$. Once again we point out that this two-particle state is a *sum* (not a product) of two single-particle states and depends only on the single variable z (and not z_1 and z_2).

In order to extract the correct sign of the charge and current density associated with the electronic and positronic portions of the "single-particle" wave function, we have to separate out states of positive and negative energy subspaces. We used the energy "filter" operator, defined as $\Lambda_u \equiv (1 + h_0/|h_0|)/2 = \Sigma_p |u;p\rangle\langle u;p|$ and $\Lambda_d \equiv (1 -$

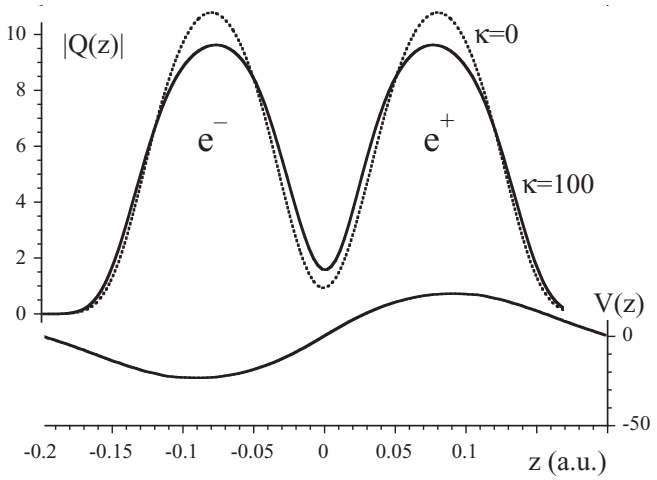

FIG. 2. The final spatial probability density of an electron (left) and positron wave packet (normalized to 2) interacting via their own internal electric field. For comparison, the dashed line represents the final density without any coupling. The potential $V(z,t)$ responsible for the attraction is shown below. (Parameters are $L = 0.4$ a.u., $N_z = 128$, $\Delta z_0 = 0.01$ a.u., $z_0 = 0.08$ a.u., $t = 0.1/c$.)

$h_0/|h_0|)/2 = \Sigma_p |d;p\rangle\langle d;p|$, where h_0 is the Hamiltonian of Eq. (2.1) without the potentials and $|h_0|$ denotes the operator $|h_0| \equiv [m^2c^4 + c^2p^2]^{1/2}$. Obviously, for any momentum p we have $\Lambda_u|u;p\rangle = |u;p\rangle, \Lambda_u|d;p\rangle = 0$, $\Lambda_d|u;p\rangle = 0$ and $\Lambda_d|d;p\rangle = |d;p\rangle$ as desired. The application of these operators can be performed quite conveniently in Fourier space. In order to get physically meaningful results from the wave function $\Phi \equiv \langle z|\Phi(t)\rangle$, we have to use the charge and current densities

$$Q(z,t) \equiv -[\Lambda_u\Phi]^\dagger\Lambda_u\Phi + [\Lambda_d\Phi]^\dagger\Lambda_d\Phi, \tag{3.3a}$$

$$J(z,t) \equiv -c[\Lambda_u\Phi]^\dagger \cdot \sigma_1\Lambda_u\Phi + c[\Lambda_d\Phi]^\dagger \cdot \sigma_1\Lambda_d\Phi \tag{3.3b}$$

in the Maxwell equations. We have noted already above that these source terms are invariant under charge conjugation, so we can omit its application here.

By comparing the final density $|\Phi(z)|^2$ with that of the uncoupled one ($\kappa = 0$), we can see the impact of the three forces. Each packet itself widens under the repulsive self-interaction while the centers of both packets move towards each other, as a consequence of the attractive force between the electron and positron (see Fig. 2). As we have now established that it is possible to model the correct interactions, we can now turn to the much more complicated quantum field theoretical problem of pair creation.

IV. PAIR CREATION WITH AND WITHOUT INTERFERMIONIC FORCES

A. Methodology

Our simulations described in the prior sections were for parameters where the total number of involved particles was conserved. We will now discuss how we can incorporate the coupling to the Maxwell equations into the pair-creation process, where the total number of particles changes and therefore requires a quantum field theoretical framework. As we discussed in the introduction nearly all works on pair creation neglected the interfermionic forces. In these calculations, the theoretical description is consistent with the Dirac sea formalism, where the quantum field theoretical vacuum is represented by a peculiar multiparticle state where each mode (single-particle state) is in a different state, such that each possible negative energy continuum state of the Hilbert space is excited exactly once. In the usual second-quantization procedure of a fermionic system, the expansion coefficients b_p of a general Dirac state $\Sigma_p[b_p(u)|u;p\rangle + b_p(d)\,|d;p\rangle]$ are replaced with anticommuting operators such that $[b_p, b^\dagger_{p'}]_+ = \delta_{p,p'}$. As a second step one associates the operators $b_p(d)$ with the creation of positrons and renames them conveniently $b_p(d) \equiv d^\dagger_{-p}$ while $b_p(u) \equiv b_p$ annihilate electrons. This step leads to a different interpretation of the states $|d;p\rangle$ than discussed in the prior quantum-mechanical sections. In other words, this initial state is given by the product of all initially occupied eigenstates associated with the negative energy continuum, $|\Phi(t=0)\rangle = \Pi_i\,|d;p_i\rangle$, where the ith particle (mode) is in the state $|d;p_i\rangle$ as defined in Eq. (2.2b) as the energy eigenstates of the free Dirac Hamiltonian h_0 with negative energy and index $i = 1,2, \ldots N$ numerates the modes (single-particle states). In the absence of interparticle interactions, the initial and final total N-particle Hamiltonian h is simply the direct sum of the Hamiltonians for each mode, $h = \Sigma h_i$, where the index i labels again each mode. The time-dependent single-mode solutions denoted by $|d;p(t)\rangle$ are obtained from the solution $i\,\partial/\partial t\,|\phi\rangle = h(e^-)\,|\phi\rangle$, where $|\phi(t=0)\rangle = |d;p\rangle$ and the Hamiltonian h takes the form of Eq. (2.1) in its spatial representation. Each of these states $|\phi(t=0)\rangle = |d;p\rangle$ is then evolved *independently* of the other modes in time, $|\Phi(t)\rangle = \Pi_i\,|d;p_i(t)\rangle$. An (upward) transition to positive energies is interpreted in the usual picture of the Dirac sea as the generation of an electron-positron pair. The number of created particle pairs $N(t)$ is then determined by the expectation value of the operator $\Sigma_i\ \Sigma_p\,|u;p_i\rangle\langle u;p_i|$, where the operator $\Sigma_p|u;p_i\rangle\langle u;p_i|$ removes the negative energy portions of the ith mode and acts as a unit operator on the other modes,

$$\begin{aligned} N(t) &= \langle\Phi(t)|\Sigma_i\Sigma_P|u;p_i\rangle\langle u;p_i||\Phi(t)\rangle \\ &= \Sigma_i\Sigma_p\Pi_i\langle d;p_i(t)||u;p_i\rangle\langle p_i||d;p_i(t)\rangle \\ &= \Sigma_{i'}\Sigma_p|\langle u;p_{i'}|d;p_i(t)\rangle|^2. \end{aligned} \tag{4.1}$$

As the dynamics were assumed to be fully decoupled between the different modes, it is not surprising that the total number of created electrons (=particle pairs) is simply the sum of all scalar products between the time evolved modes $|d;p(t)\rangle$ and all single-particle states with positive energy $|u;p\rangle$. As was shown numerous times in the literature [15,41], this expression is identical to the one obtained from quantum field theory. In other words, all aspects of the above multiparticle quantum-mechanical description are identical to a full quantum field theory in the case where the interfermionic forces can be neglected.

As indicated in the introduction, all quantum field theoretical approaches to pair creation assume that the initially occupied negative energy eigenstates (Dirac sea) are depleted independently from each other due to the external potential. In an energy discretized (and truncated) numerical description,

we assume that the negative energy portion of the Hilbert space is spanned by a total of N_z states. The parameter N_z is also identical to the number of spatial grid points.

As an initially occupied negative energy state represents parts of the neutrally charged quantum field theoretical vacuum, we have to guarantee that each initial Dirac sea state does not contribute to the charge and current source terms in the Maxwell equation. The pair-creation induced "holes" in the negative energy states (=created positrons) correspond to the positive charge in the Maxwell equation.

B. Numerical results

Similarly as in many prior works [41], we have used the Sauter potential well [42] of the form

$$V_{\rm ext}(z) = V_0\{\tanh[(z + D/2)/W] + \tanh[(D/2 - z)/W]\}/2 \tag{4.2}$$

with an amplitude V_0, a spatial extension D, and spatial width W to model the external supercritical field and use $A_{\rm ext} = 0$. It satisfies the required periodic boundary conditions and permits us to explore two pair-creation zones centered at $z = \pm D/2$, where the external force is largest. Due to the short-range character of this potential, the (long-time) charge density associated with this potential $[\rho(z) = -\partial_z^2 V_{\rm ext}/(4\pi)]$ would have two maxima and minima, reflecting a vanishing total charge. This charge density is therefore different from the one associated with a single supercritical positively charged nucleus. The total charge under each maximum is approximately $V_0/(8\pi W)$ which amounts to the rather large charge of 6×10^5 a.u. for our parameters ($V_0 = 3c^2$, $W = 0.5/c$) taken in our simulations below. If the created electron-positron pair were to interact with the coupling strength $\kappa = 1$, the corresponding force between both particles would be negligable in this gigantic external charge cloud.

In order to avoid any sudden population burst due to a too abrupt turn-on, we have increased the amplitude smoothly to $V_0 = 3c^2$ with the function $\sin^2[\pi t/(2T_{\rm on})]$ during the early time interval $0 < t < T_{\rm on}$. We chose $T_{\rm on} = 0.01/c$ in most calculations.

To give the reader a brief summary of the numerical convergence of the algorithm and the scaling of the total user cpu time with the size of the space-time grid, we show the final number of created particle pairs for various numerical parameters in Table I. Similarly as in our simulations below we used $V_0 = 3c^2$, $W = 0.5/c$, $D = 0.2$ a.u., $\kappa = 300$ and examined a total interaction time of $T = 0.1/c$ on a spatial grid of total length $L = 0.4$ a.u. We note that the interaction time (and the unusal unit system) was chosen such that a particle (or field) that evolves with the speed of light c could cover a distance 0.1 a.u., which is the separation between the center of our force creation zone and the right edge of our numerical box.

For simplicity, we ran the simulation on just 16 processors of a 2.6-GHz Dell PowerEdge R815. The user execution times per processor are comparable to those runs performed on a 2.26-GHz Macintosh Pro. It should be clear that the total cpu time used for the time evolution scales roughly linearly in N_t while the underlying algorithms for the fast Fourier transformations (FFTs) are the principle bottleneck of the code and determine the scaling with N_z. The accuracy and the rather short execution times for even large grids with small N_t and N_z suggest that the code might become computationally feasible in the future also in two (or possibly even three) spatial dimensions.

TABLE I. The total number of created electron-positron pairs for simulations with various number of spatial (N_z) and temporal (N_t) gridpoints for the FFT-based Dirac and Maxwell algorithm. For comparison, for $\kappa = 0$ we find $N(t) = 1.1316$. (Parameters are $L = 0.4$ a.u., $T = 0.1/c$, $\kappa = 300$, $V_0 = 3c^2$, $W = 0.5/c$, $D = 0.2$ a.u., $E_{\rm cut} = 7.3c^2$.)

N_z	N_t	cpu time (s)	No. pairs $N(t)$
128	1000	102	1.2479
256	1000	278	1.2360
512	1000	768	1.2360
1024	1000	2956	1.2360
256	50	14	1.1977
256	100	27	1.2218

In order to have confidence in the correct implementation of the algorithm it is also important to check the scaling of the numerical error associated with the finite size of the space-time lattice. As a measure for the convergence of the code we have considered here the deviation of the final number of created electron-positron pairs N from the one obtained from a simulation with the smallest temporal grid spacing Δt (associated with the largest number of temporal steps N_t). In Fig. 3 we show this error scaling using doubly logarithmic axis, where we have decreased $\Delta t = 2.92 \times 10^{-5}$ a.u (associated with only $N_t = 25$ temporal steps) to $\Delta t = 9.13 \times 10^{-7}$ a.u. (associated with $N_t = 800$). The comparison with the reference line that has the exact slope 2 shows that the global error of our code scales quadratically with Δt, fully consistent with

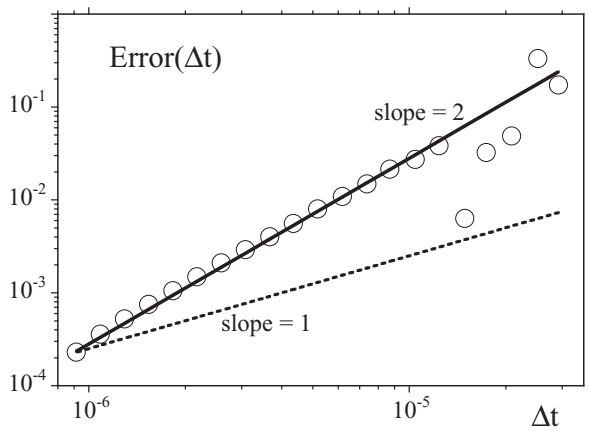

FIG. 3. The scaling of the global error $\text{Error}(\Delta t) \equiv |N(\Delta t) - N_{\rm exact}|$ associated with the final number of created electron-positron pairs N as a function of 21 temporal grid spacings $\Delta t = T/N_t$ used in each simulation. As a reference value for $N_{\rm exact} = 1.236\,130\,006$ we used here the number of created pairs computed from the simulation with the smallest time step ($\Delta t = T/1600$). The two reference lines are $\text{Error}(\Delta t) = 10^{8.45}\ \Delta t^2$ and $\text{Error}(\Delta t) = 10^{2.4}\ \Delta t$ (dashed). (Parameters are $L = 0.4$ a.u., $T = 0.1/c$, $\kappa = 300$, $V_0 = 3c^2$, $W = 0.5/c$, $D = 0.2$ a.u., $N_z = 256$, $E_{\rm cut} = 7.3c^2$.)

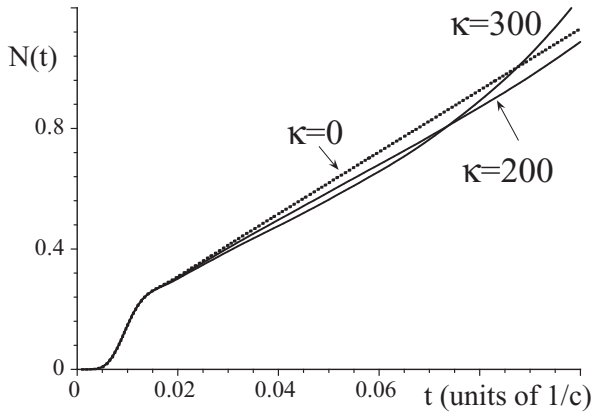

FIG. 4. The total number of created electron-positron pairs $N(t)$ as a function of time t for three coupling strengths κ of the interfermionic forces. (Parameters are $L = 0.4$ a.u., $N_z = 512$, $N_t = 1000$, $V_0 = 3c^2$, $W = 0.5/c$, $D = 0.2$ a.u., $E_{\rm cut} = 7.3c^2$.)

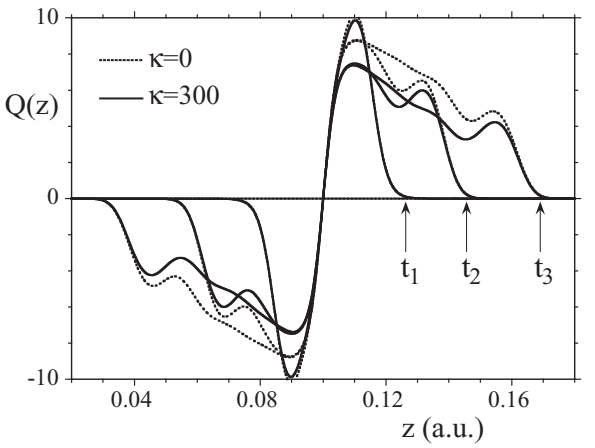

FIG. 5. Snapshots of the charge density $Q(z,t)$ (top) at three different times ($t_n = n0.025/c$ with $n = 1,2,3$). For comparison, the dashed lines are the density in the absence of the interfermionic force ($\kappa = 0$). (Parameters as in Fig. 4, except $N_t = 900$.)

a local error $O(\Delta t^3)$ as expected and derived in Appendix B for this FFT based code. We used a spatial grid with $N_z = 256$ grid points. And the data are graphically indistinguishable with the data for $N_z = 512$, as already suggested by Table I. For example, for $\Delta t = T/1600$ we obtain $N = 1.236\,130\,006$ for $N_z = 256$ while for $N_z = 512$ we got $N = 1.236\,130\,001$.

Let us now analyze the physical impact of the interfermionic forces on the pair-creation process. In Fig. 4 we compare the time dependence of the number of created pairs $N(t) = \Sigma_p \langle\langle \text{vac}||b_p^\dagger(t)b_p(t)||\text{vac}\rangle\rangle$ with ($\kappa = 200$ and 300) and without ($\kappa = 0$) the interfermionic forces. We see that at very early times internal forces play no role and all three curves match. This is consistent with the finding that the electrons and positrons are being created "on top of each other" [43] such that the initial charge density remains zero. If the initial birth velocities of both particles were equally distributed, the early time current density vanishes as well. Only at later times when the particles are accelerated in the supercritical field do the interfermionic potentials grow.

In the next time regime ($0.02/c < t < 0.07/c$) we see that the interfermionic forces suppress the yield; the larger the coupling κ, the smaller actually is the number of created pairs. This could be consistent with the general expectation that it is more difficult to create (and separate) particles that mutually attract. At even longer times ($t > 0.07/c$ for $\kappa = 300$) the mutual attraction leads to an increase of the pair creation yield. We also see that the onset time of this pair-creation enhancement decreases with increasing coupling κ.

Below we will now illuminate this process from a spatial perspective by computing the charge density $[Q(z,t)]$, the internal scalar $[V(z,t)]$ and vector potential $[A(z,t)]$ as well as the spatial probability distribution of the electrons $[\rho(e^-;z,t)]$ and positrons $[\rho(e^+;z,t)]$. The total charge and current densities are usually calculated from the expectation value of the corresponding operators as

$$Q(z,t) \equiv \langle \text{vac}|q[\Psi(z,t)^\dagger\Psi(z,t) - \Psi(z,t)\Psi(z,t)^\dagger]/2|\text{vac}\rangle, \tag{4.3a}$$

$$J(z,t) \equiv \langle \text{vac}|qc[\Psi(z,t)^\dagger\sigma_1\Psi(z,t) - \Psi(z,t)\sigma_1\Psi(z,t)^\dagger]/2|\text{vac}\rangle. \tag{4.3b}$$

The total charge and current densities defined in Eq. (4.3a) and (4.3b) contain also the propagation of the vacuum's polarization density associated with the external potential $V_{\rm ext}(z)$ as we illustrate in Appendix C. As we want to focus in this study solely on the effect of the electron-positron force on the pair-creation process, we have used only the particle-pair induced charge and current densities as source terms in the Maxwell equation. This density based on the difference between the positronic and electronic mass densities $Q(z,t) = \rho(e^+;z,t) - \rho(e^-;z,t)$, as defined below.

In Fig. 5 we show the time evolution of the charge density $Q(z,t)$. For reasons of symmetry, we focus only on the right pair-creation zone around $z = 0.1$ a.u. At each moment the spatial integral over $Q(z,t)$ vanishes, reflecting the expected conservation of the total charge $\int dz\, Q(z,t) = 0$. As mentioned above, at the spatial location $z = 0.1$ a.u. (where the force given by the gradient of the external potential is maximum) most of the particles are created. In the absence of any interfermionic forces, the positrons are ejected mainly to the right (and correspondingly to the left from $z = -0.1$ a.u), while the corresponding electrons are accelerated in the opposite direction. The simulation results in the absence of any interferminic forces ($\kappa = 0$) are indicated by the dashed lines. For example, for 0.1 a.u. $< z$ we see that the internal forces are responsible for a clear reduction of the total charge density. This could either be associated with a reduction of the number of created positrons or the occurrence of electrons that neutralize the charge locally. The first mechanism would certainly contradict the observed increase of the created number of pairs at a later time. The corresponding current density can be obtained from the continuity equation and is consistent with the findings of the charge density and does not necessarily provide us with additional information about the dynamics.

In Fig. 6 we show how the birth of charged particles is directly associated with the birth of the corresponding force

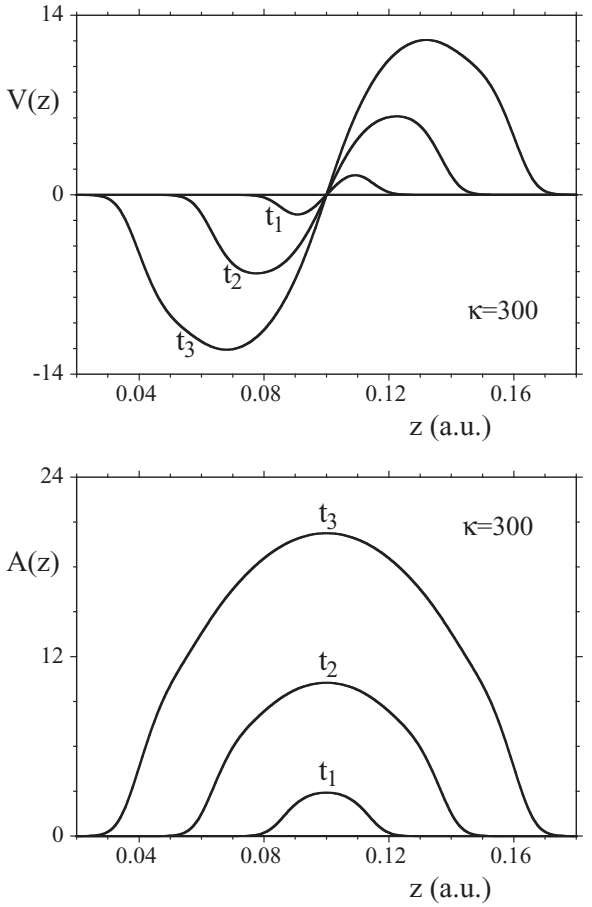

FIG. 6. Snapshots of the created internal scalar $V(z,t)$ (top) and vector $A(z,t)$ potential (bottom) at the same times as in Fig. 5. (Parameters as in Fig. 5.)

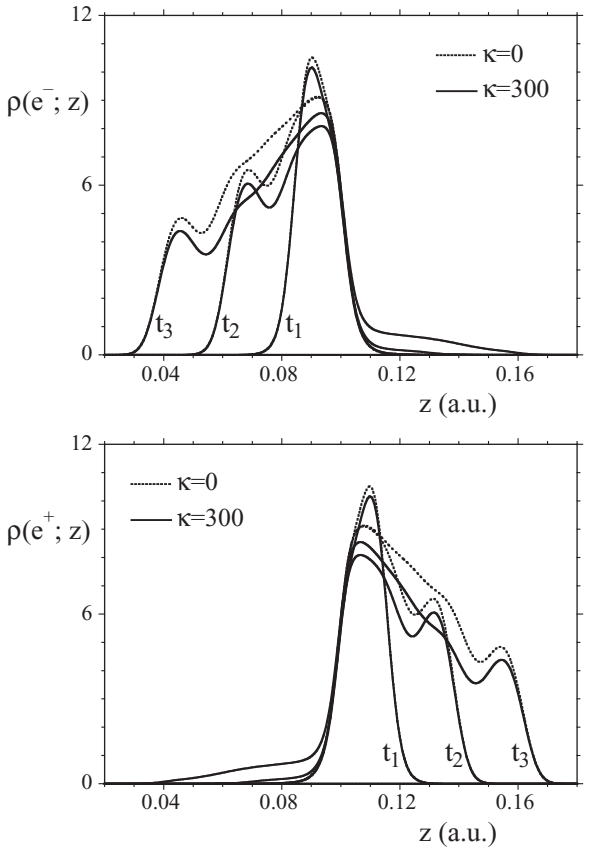

FIG. 7. Snapshots of the spatial probability density of the created electrons $\rho(e^-;z,t)$ (top) and positrons $\rho(e^+;z,t)$ (bottom) with and without (dashed lines) the interfermionic forces. (Parameters as in Fig. 4.)

field between them. While the velocity of massive particles is below the speed limit c, their created scalar vector potentials evolve with the speed of light c. We might add here that once the internal potentials reach the boundaries of our numerical box, the simulation data become more difficult to interpret due to the assumed periodic boundary.

The charge density $Q(z)$ does not allow us to distinguish between the density of the individual electrons and positrons. For example, if an electron and a positron have identical spatial probability densities, then the total charge density is zero, as if there were no particles at all. It is also therefore not possible to compute the total number of created electron-positron pairs directly from $Q(z)$. In order to be able to distinguish both cases, we have to compute also a spatial probability density for each type of particle. Consistent with prior works [41], we propose here to define spatial probability densities that are based on the assumption that we can separate the total electron-positron field operator into a positronic and electronic portion. These two densities can be obtained from the expectation value of the corresponding electronic $[\Psi(e^-;t)]$ and positronic $[\Psi(e^+;t)]$ portion of the total field operator $\Psi(t) = \Psi(e^-;t) + C_{\rm op}\,\Psi(e^+;t)$. We obtain $\psi(e^-;t) \equiv \Lambda_u\,\Psi$ and $\Psi(e^+;t) \equiv \Lambda_u C_{\rm op}\,\Psi\,C_{\rm op}$, where $C_{\rm op}$ is the quantum field theoretical generalization of the charge-conjugation operator C. This definition of $\Psi(e^-;t)$ and $\Psi(e^+;t)$ allow us to compute the total number of particles,

$$\rho(e^-;z,t) \equiv \langle {\rm vac}|\Psi(e^-;z,t)^\dagger\Psi(e^-;z,t)|{\rm vac}\rangle, \quad (4.4a)$$

$$\rho(e^+;z,t) \equiv \langle {\rm vac}|\Psi(e^+;z,t)^\dagger\Psi(e^+;z,t)|{\rm vac}\rangle. \quad (4.4b)$$

Here it is important to note that the total charge operator $q[\Psi^\dagger\Psi - \Psi\Psi^\dagger]/2$ [of Eq. (4.3a)] and the "particle pair-induced" operator $q[\Psi(e^-)^\dagger\Psi(e^-) - \Psi(e^+)^\dagger\Psi(e^+)]$ are not necessarily identical if the vacuum's polarization charge density due to the fact that the external potential is large. We note that for consistency the area under each curve $\rho(e^-;z,t)$ is identical to the number of particles. We also refer to the literature [44,45] for a more careful description of how these densities have to be interpreted in the region where the external field is supercritical. We should note that an unambiguous identification of electrons and positrons inside the pair-creation zone is still a major unresolved problem in theoretical physics.

Finally, in Fig. 7 we show the spatial probability distribution of each particle species, denoted by $\rho(e^\pm;z,t)$. The pair-creation suppression observed for early times in Fig. 4 finds its direct confirmation in the spatial density. While for early times the electronic densities $\rho(e^-;z,t_1)$ with and without the coupling are similar at later times, the density for $\kappa = 300$ is less than the one without any internal interaction. The electrons ejected to the left side of the right creation zone at $z = 0.1$ a.u. attract the ejected positrons escaping to the right. As a result we

find less probability close to the front edge of the distribution. While some positrons cannot flow out of the creation zone so efficiently, they reduce the creation of additional positrons due to Pauli blocking [46–48]. The density close the creation zone therefore also decreases.

The second and third temporal snapshot show that the unique assignment of each spatial region with a specific charge is no longer possible due to the internal forces. The interaction $\kappa = 300$ leads to the occurrence of electrons on the right side (0.1 a.u $< z$) of the pair-creation zone. In fact, the occurrence of electrons in the region $z > 0.1$ a.u. is fully consistent with the reduction in the charge observed above in Fig. 5. The density at t_3 shows the modification of the pair-creation yield due to the interaction. A more detailed analysis of the spatial implications of the internal forces is beyond the framework of the present work and will be examined in future studies.

V. SUMMARY AND OUTLOOK

The purpose of this work was twofold. First, we outlined a theoretical and also computational procedure that permits us to include the effects of the electron-positron, electron-electron, and positron-positron interactions into the pair-creation process. This was done on an approximate level where the second-quantized character of the force intermediating bosonic field was neglected and the photons were approximated by a classical field whose time evolution is given by the Maxwell equations. Second, we used this framework under the simplifying situation of only one spatial dimension to show that the attractive and repulsive character of the Coulombic interaction can be correctly described. Furthermore we obtained some preliminary data on the effect of the Maxwell equations on the pair-creation process. The availability of this approach permits us now to tackle several new challenges for future studies, five of which we briefly outline below.

We have shown that the absence of the second quantization leads unavoidably to an unphysical self-repulsion of a single free particle. By comparing the effect on the enhancement of wave packet spreading with those of a classical ensemble of fully interacting charged quasiparticles [49,50] in the relativistic regime, we will obtain a better estimate of the magnitude (and therefore dynamical relevance) of this effect. It is presently not clear if this effect is intrinsically quantum mechanical or can be fully explained in terms of classical mechanics. A better understanding of the self-repulsion mechanism would also help us to distinguish it from the physically relevant (multiparticle) repulsion between two equally charged particles.

As the proposed computational algorithm is fully parallelizable we expect that the generalization of this approach to two (and possibility even three) spatial dimensions and four spinor-component Dirac states could be feasible. In this case it might be interesting to learn about the relevance of the spin and its coupling to the fields for the pair creation, which could not be studied in a reduced dimensional system.

As the system and all interactions are fully relativistic, all retardation effects and the back reaction of the particles onto the fields are included. It might be interesting to compare two-particle interactions on a level where they are approximated by a simple instantaneous Coulomb force without the feedback onto the fields. Furthermore, using a simplified Yukawa model system, some recent work [51] has suggested how this interaction is modified if the boson field is second quantized and the true absorption and emission of photons are included.

For longer interaction time $t > D/c$ it is well known [52,53] that the pair creation due to a finite well will eventually come to a complete halt, associated with the creation of the fully occupied trapped states. Due to the Pauli exclusion principle, the captured electrons block a further pair creation. We have seen in Fig. 7 that due to the interfermionic forces also positrons can occur inside the well. It is therefore very interesting to monitor their impact on Pauli blocking and the formation of the trapping states.

In order to focus exclusively on the effect of the forces between the charges we have separated in this work the force fields into external supercritical and internal ones. Similarly to a recent study by the group in Heidelberg [12,13], one can also assume that there is no externally given force field and include all forces into the Maxwell dynamics. In this case we have total-energy conservation and one can observe how the initial field energy is converted to create particles.

ACKNOWLEDGMENTS

We thank Dr. S. Ahrens, Dr. J. Dallon, Dr. C. C. Gerry, Dr. S. Glasgow, Dr. A. Harris, and Dr. F. Hebenstreit for useful discussions and S. Norris and A. Vikartofsky for help regarding the parallelization of the code. We especially appreciate a visit by Dr. F. Hebenstreit to our group. This work has been supported by the NSF and the NSFC (Grant No. 11128409). It also used the Extreme Science and Engineering Discovery Environment *(XSEDE)*, which is supported by NSF Grant No. OCI-1053575.

APPENDIX A: THE HAMILTONIAN FOR ONE-DIMENSIONAL QED

In one spatial dimension the covariant form of the QED Lagrangian density [54–57] is given by

$$L(z,t) = \Psi_b \sigma_3 [i\hbar\partial_t - c\sigma_1 p - \sigma_3 mc^2]\Psi + (1/8\pi)(\partial_z V + \partial_{ct} A)^2 - q\,\Psi_b(\sigma_3 V - i\sigma_2 A)\Psi, \tag{A1}$$

where σ_i denotes again the Pauli matrices, $\Psi_b \equiv \Psi^\dagger \sigma_3$ is the adjoint electron-positron field, and $V(z,t)$ and $A(z,t)$ are the total scalar and vector potentials. The coupling q is the charge, which we put equal to -1 a.u. in atomic units. Except the prefactor $(1/8\pi)$ in front of the field energy, the Lagrangian can be derived from the three-dimensional form if we identify the usual γ matrices as $\gamma^0 = \sigma_3$ and $\gamma^1 = i\sigma_2$. This arbitrary choice for the γ matrices has been made such that the resulting Dirac equation matches the one frequently studied in the past [41]. The electric field is given from the potentials as $E(z,t) = -(\partial_z V + \partial_{ct} A)$. It is equal to the (0,1) component of the antisymmetric electric-field tensor, which has only two nonvanishing components.

The Dirac and Maxwell equations follow directly from the corresponding Euler-Lagrange equations, which minimize the

corresponding action integral,

$$\partial_{ct}[\partial L/\partial(\partial_{ct}\phi)] + \partial_z[\partial L/\partial(\partial_z\phi)] - \partial L/\partial\phi = 0. \quad \text{(A2)}$$

Here the place holder symbol ϕ represents either Ψ_b, A, or V. For example, using $\phi = \Psi_b$ the first two terms $\partial L/\partial(\partial_{ct}\Psi_b)$ and $\partial L/\partial(\partial_z\Psi_b)$ vanish, as L does not depend on any spatial or temporal derivative of the adjoint field. Using $\sigma_3\sigma_2 = -i\sigma_1$ we obtain

$$\partial L/\partial\phi = \sigma_3[i\hbar\partial_t - c\sigma_1(p - qA/c) - \sigma_3 mc^2 - qV]\Psi = 0, \quad \text{(A3)}$$

which is the time-dependent Dirac equation $[i\hbar\partial_t - h]\Psi = 0$ where $h \equiv c\sigma_1(p - qA/c) + \sigma_3 mc^2 + qV$. Furthermore, using $\phi = \mathrm{V}$ the term $\partial L/\partial(\partial_{ct}V)$ vanishes and we obtain

$$\partial_z[\partial L/\partial(\partial_z V)] = \partial_z(1/4\pi)(\partial_z V + \partial_{ct}A) = -(1/4\pi)\partial_z E, \quad \text{(A4a)}$$

$$\partial L/\partial V = -q\Psi_b\sigma_3\Psi = -q\Psi^\dagger\Psi, \quad \text{(A4b)}$$

which leads immediately to Gauss's law $\partial_z E = 4\pi q\Psi^\dagger\Psi$. The second Maxwell equation follows if we use $\phi = A$. Using that $\partial L/\partial(\partial_z A) = 0$ we obtain

$$\partial_{ct}[\partial L/\partial(\partial_{ct}A)] = \partial_{ct}(1/4\pi)(\partial_z V + \partial_{ct}A) = -(1/4\pi)\partial_{ct}E, \quad \text{(A5a)}$$

$$\partial L/\partial A = q\Psi_b i\sigma_2\Psi = q\Psi^\dagger\sigma_1\Psi \quad \text{(A5b)}$$

leading to the equation $\partial_t E = -4\pi cq\Psi^\dagger\sigma_1\Psi$.

In order to examine the energy balance between the electrons, positrons, and the electric field, we have to reconstruct QED in its Hamiltonian formulation. To do so we have to find first the corresponding canonical momenta to the three fields. We obtain

$$\Pi_\Psi = \partial L/(\partial_{ct}\Psi) = \Psi_b ci\hbar\sigma_3, \quad \text{(A6a)}$$

$$\Pi_A = \partial L/(\partial_{ct}A) = (1/4\pi)(\partial_z V + \partial_{ct}A), \quad \text{(A6b)}$$

$$\Pi_V = \partial L/(-\partial_{ct}V) = -(1/4\pi)(\partial_z V + \partial_{ct}A). \quad \text{(A6c)}$$

If we apply the Legendre transformation to the Lagrangian density we obtain

$$\begin{aligned} H(z) &= \Pi_\Psi\partial_{ct}\Psi + \Pi_A\partial_{ct}A + \Pi_V(-)\partial_z V - L \\ &= \Psi_b\sigma_3[c\sigma_1(p - qA/c) + \sigma_3 mc^2 + qV]\Psi \\ &\quad + (1/8\pi)(\partial_z V + \partial_{ct}A)^2. \end{aligned} \quad \text{(A7)}$$

While the original fields commute with each other, the quantum field operators do not; we therefore replace the Hamiltonian here by a form for which the fermionic degrees of freedom are antisymmetrized for any possible exchange of the operators,

$$H(z) = [\Psi_b\sigma_3, h\Psi]/2 + (1/8\pi)(\partial_z V + \partial_{ct}A)^2. \quad \text{(A8)}$$

Similarly, we also introduce the total charge and current density operators as $Q \equiv q[\Psi^\dagger,\Psi]/2$ and $J \equiv cq[\Psi^\dagger,\sigma_1\Psi]/2$. Using the Hamiltonian density from Eq. (A8) we can construct the total Hamiltonian $H \equiv \int dz H(z)$.

As a side issue, we should mention [58] that by applying the Heisenberg equations of motion to the Hamiltonian $i\hbar\partial\phi/\partial t = [\phi, H]$, we recover the time-dependent equations of motion

$$i\hbar\partial E/\partial t = [E,H] \Rightarrow \partial E/\partial t = -4\pi J, \quad \text{(A9a)}$$

$$i\hbar\partial A/\partial t = [A,H] \Rightarrow \partial A/\partial t = -cE - c\partial V/\partial z, \quad \text{(A9b)}$$

$$i\hbar\partial\Psi/\partial t = [\Psi,H] \Rightarrow i\hbar\partial\Psi/\partial t = h\Psi. \quad \text{(A9c)}$$

In the first equation we have used that the pairs of canonical variables fulfill the anticommutator $[\Psi_i,\Psi_j^\dagger]_+ = \delta_{i,j}\delta(z - z')$ and commutator relationship $[E,A] = 4\pi i\delta(z - z')$. We also used that $[A,BC] = [A,B]_+C - B[A,C]_+$. As H is only the generator of the time evolution, it should be clear that Gauss's law cannot be derived from a Hamiltonian formalism alone. However, one can show that if the initial fields satisfy $\partial_z E(t = 0) = 4\pi q\Psi^\dagger(t = 0)\Psi(t = 0)$, then this equation will be automatically fulfilled at all later times as well [58]. In this sense the Hamiltonian formalism is equivalent to the Lagrangian formulation.

APPENDIX B: NUMERICAL ALGORITHM

The solution to the time-dependent Dirac equation with the Hamiltonian $h = h_0 + h_{\mathrm{int}}$,

$$h_0 \equiv c\sigma_1 p + \sigma_3 c^2, \quad \text{(B1a)}$$

$$h_{\mathrm{int}} \equiv -\sigma_1\kappa qA(z,t) - \sigma_1 qA_{\mathrm{ext}}(z,t) + \kappa qV(z,t) + qV_{\mathrm{ext}}(z), \quad \text{(B1b)}$$

is standard by now and we use the well-documented FFT based split-operator algorithm for this [23–26]. Here the action of the force-free part h_0 is performed in Fourier space, while the action of the second portion h_{int} can be efficiently done in coordinate space.

As solution techniques to the Maxwell equation are not so well documented [59], we summarize here the essential steps of our algorithm. It is based on the fact that for a given inhomogeneity, the wave equation can be solved exactly, so it just needs to be sampled on our given space-time grid. If we abbreviate our notation below for time t as $F_1(z) \equiv A(z,t)$ and $F_2(z) \equiv \partial_t A(z,t)$, the Maxwell equation

$$\left(\partial_{ct}^2 - \partial_z^2\right)A(z,t) = 4\pi c^{-1}\kappa J(z,t) \quad \text{(B2)}$$

has an exact solution given by the sum of three terms. The first two terms T_1 and T_2 are solutions to the homogeneous wave equation, while the third term T_3 depends on the source term:

$$A(z,t + \Delta t) = T_1 + T_2 + T_3, \quad \text{(B3)}$$

$$T_1 \equiv [F_1(z + c\Delta t) + F_1(z - c\Delta t)]/2, \quad \text{(B3a)}$$

$$T_2 \equiv 1/(2c)\int_{z-c\Delta tz}^{z+c\Delta tz} dz' F_2(z'), \quad \text{(B3b)}$$

$$T_3 \equiv (c/2)\int_t^{t+\Delta t} dt' \times \int_{z-c(t+\Delta t-t')}^{z+c(t+\Delta t-t')} dz' 4\pi c^{-1}\kappa J(z',t'). \quad \text{(B3c)}$$

We need to implement this analytical solution for one time step Δt on the same space-time grid as used for the wave-function calculations. In order to obtain the correct

second time derivative of F_1, we need to update $F_1(z+c\Delta t)$ from $F_1(z)$ accurately to at least $O(\Delta t^2)$. Below we use the usual (three-point) quadratic interpolation approximation $f(z) \approx \Sigma_{i=1}^{3} f(z_i)\,\Pi_{j=1}^{3}(z-z_j)/(z_i-z_j)$, where the factor $(z-z_i)/(z_i-z_i)$ associated with the special index $j=i$ is omitted in the product. For the first term in Eq. (B3) $[F_1(z+c\Delta t)+F_1(z-c\Delta t)]/2$, we obtain

$$\begin{aligned} T_1 &= (c\Delta t)^2/(2\Delta z^2)F_1(z-\Delta z) \\ &\quad + [1-(c\Delta t)^2/\Delta z^2]F_1(z) + (c\Delta t)^2/(2\Delta z^2)F_1(z+\Delta z) \\ &\quad + O(\Delta t^3). \end{aligned} \tag{B4}$$

For the second term, use the same interpolation for the integrand $F_2(z')$, based on our grid points $z-\Delta z$, z, and $z+\Delta z$,

$$\begin{aligned} F_2(z') &= F_2(z-\Delta z)[z'-z][z'-(z+\Delta z)]/(2\Delta z^2) \\ &\quad + F_2(z)[z'-(z-\Delta z)][z'-(z+\Delta z)]/(-\Delta z^2) \\ &\quad + F_2(z+\Delta z)[z'-(z-\Delta z)][z'-z]/(2\Delta z^2) \\ &\quad + O(\Delta z^3). \end{aligned} \tag{B5}$$

We obtain

$$\begin{aligned} T_2 &= 1/(2c)\int_{z-c\Delta t}^{z+c\Delta t} dz' F_2(z') \\ &= c^2\Delta t^3/(6\Delta z^2)F_2(z-\Delta z) \\ &\quad + [\Delta t - c^2\Delta t^3/(3\Delta z^2)]F_2(z) \\ &\quad + c^2\Delta t^3/(6\Delta z^2)F_2(z+\Delta z) + O(\Delta z^3). \end{aligned} \tag{B6}$$

Finally, the first integrand in the third term T_3 and abbreviated as $I_3(t,t') = \int_{z-c(t+\Delta t-t')}^{z+c(t+\Delta t-t')} dz'\,4\pi c^{-1}\kappa J(z',t')$ can be interpolated using the grid points at $z-\Delta z$, z, and $z+\Delta z$,

$$\begin{aligned} I_3(t') &= \int_{z-c(t+\Delta t-t')}^{z+c(t+\Delta t-t')} dz' 4\pi c^{-1}\kappa J(z',t') \\ &= 4\pi c^{-1}\kappa\{[c(t+\Delta t)-ct']^3/(3\Delta z^2)J(z-\Delta z,t') \\ &\quad + 2[c(t+\Delta t)-ct']J(z,t') \\ &\quad - 2[c(t+\Delta t)-ct']^3/(3\Delta z^2)J(z,t') \\ &\quad + [c(t+\Delta t)-ct']^3/(3\Delta z^2)J(z+\Delta z,t')\}. \end{aligned} \tag{B7}$$

In order to force the remaining temporal integral $(c/2)\int_t^{t+\Delta t} dt' I_3(t')$ onto our temporal grid, we approximate the current density in the integrand at each spatial grid point by a two-point formula, $J(t') = J(t+\Delta t)(t'-t)/\Delta t + J(t)(t'-t-\Delta t)/(-\Delta t) + O(\Delta t^2)$. Finally we obtain the six terms

$$\begin{aligned} T_3 &= (c/2)\int_t^{t+\Delta t} dt' I_3(t') \\ &= 2\alpha J(z-\Delta z,t) + (2\beta-4\alpha)J(z,t) + 2\alpha J(z+\Delta z,t) \\ &\quad + (\alpha/2)J(z-\Delta z,t+\Delta t) + (\beta-\alpha)J(z,t+\Delta t) \\ &\quad + (\alpha/2)J(z+\Delta z,t+\Delta t) + O(\Delta t^3) + O(\Delta z^3), \end{aligned} \tag{B8}$$

where $\alpha \equiv \kappa\pi c^3\Delta t^4/(15\Delta z^2)$ and $\beta \equiv 2\kappa\pi c\Delta t^2/3$.

In total, we have the sum of the results from Eqs. (B4), (B6), and (B8), giving us the final algorithm to evolve the potential a time step forward from t to $t+\Delta t$:

$$\begin{aligned} A(z,t+\Delta t) &\approx (c\Delta t)^2/(2\Delta z^2)F_1(z-\Delta z) + [1-(c\Delta t)^2/\Delta z^2]F_1(z) + (c\Delta t)^2/(2\Delta z^2)F_1(z+\Delta z) \\ &\quad + c^2\Delta t^3/(6\Delta z^2)F_2(z-\Delta z) + [\Delta t - c^2\Delta t^3/(3\Delta z^2)]F_2(z) + c^2\Delta t^3/(6\Delta z^2)F_2(z+\Delta z) \\ &\quad + 2\alpha J(z-\Delta z,t) + (2\beta-4\alpha)J(z,t) + 2\alpha J(z+\Delta z,t) \\ &\quad + (\alpha/2)J(z-\Delta z,t+\Delta t) + (\beta-\alpha)J(z,t+\Delta t) + (\alpha/2)J(z+\Delta z,t+\Delta t) + O(\Delta t^3) + O(\Delta z^3). \end{aligned} \tag{B9}$$

We also need to update $F_2(z)[=\partial_t A(z,t)]$ to $F_2(z,t+\Delta t)$ where we can use the already calculated values for $\partial_t A(z,t)$, $A(z,t)$, $A(z,t+\Delta t)$. We construct the Taylor expansions around t for $A(z,t+\Delta t)$ and $\partial_t A(z,t+\Delta t)$ up to $O(\Delta t^3)$. If we multiply the expansion for $\partial_t A(z,t+\Delta t)$ with $-\Delta t/2$ and add it to the one for $A(z,t+\Delta t)$, the common term containing the second derivative $\partial_t^2 A(z,t+\Delta t)$ cancels out. If we solve the resulting single equation for $\partial_t A(z,t+\Delta t)$ we obtain

$$\begin{aligned} \partial_t A(z,t+\Delta t) &= -\partial_t A(z,t) + A(z,t+\Delta t)2/\Delta t \\ &\quad - A(z,t)2/\Delta t + \partial_t^3 A(z,t)\Delta t^2/6 + O(\Delta t^3). \end{aligned}$$

We then truncate the third derivative term and obtain

$$F_2(z,t+\Delta t) = 2[A(z,t+\Delta t) - A(z,t)]/\Delta t - F_2(z). \tag{B10}$$

This equation allows us to update F_2 to $F_2(z,t+\Delta t)$ after we have first updated to $A(z,t+\Delta t)$ using Eq. (B9). As the terms containing F_2 in Eq. (B9) are each multiplied with a factor at least linear in Δt, the truncation $\partial_t^3 A(z,t) = 0$ has no impact on the overall accuracy of the code for A. The corresponding solution technique to the equation for the potential V, $(c^{-2}\partial_t^2 - \partial_z^2)V = 4\pi\kappa Q(z,t)$, is, of course, identical except that we have to replace J by cQ. We also note that, using the Lorenz gauge, $\partial_z A = -c^{-1}\partial_t V$, the two potentials can be converted directly into each other.

As a final remark, we should mention that a computationally more elegant, but also more cpu-time consuming algorithm to solve the Maxwell-wave equations can be obtained by Fourier transforming the field and the source term $S(z,t) = 4\pi c^{-1}\kappa J(z,t)$ or $4\pi c\rho(z,t)$ into momentum space,

$$\left(\partial_{ct}^2 + k^2\right)F(k,t) = S(k,t). \tag{B11}$$

We can use quadratic interpolation for the source term $S(k,t) \equiv S(t)$ at the three temporal grid points $s_- \equiv S(t_{n-1})$, $s_0 \equiv S(t_n)$ and $s_+ \equiv S(t_{n+1})$ and obtain for the inside interval

$t_n \leqslant t \leqslant t_{n+1}$,

$$\begin{aligned} S(t) &= s_-(t_n - t)(t_{n+1} - t)/(2\Delta t^2) \\ &\quad - s_0(t_{n-1} - t)(t_{n+1} - t)/\Delta t^2 \\ &\quad + s_+(t_n - t)(t_{n-1} - t)/(2\Delta t^2) + O(\Delta t^3) \\ &= g_0 + g_1(t - t_n) + g_2(t - t_n)^2 + O(\Delta t^3) \end{aligned} \quad \text{(B12a)}$$

with the coefficients [g_i reflecting the corresponding finite-difference formulas $g_i \equiv d^i S(t_n)/dt_n^i$]

$$\begin{aligned} &g_0 \equiv s_0, \quad g_1 \equiv (s_+ - s_-)/(2\Delta t), \\ &g_2 \equiv (s_+ - 2s_0 + s_-)/(2\Delta t^2). \end{aligned} \quad \text{(B12b)}$$

It turns out that for a quadratic source term $S(t) = g_0 + g_1(t - t_n) + g_2(t - t_n)^2$ the wave equation can be solved exactly and we obtain for time t_{n+1} the solution (for $k \neq 0$)

$$\begin{aligned} F(t_{n+1}) = {} & F(t_n)\cos[ck\Delta t] + dF(t_n)/dt_n \sin[ck\Delta t]/(ck) \\ & - 2g_2/(c^2k^4) + (g_0 + g_1\Delta t + g_2\Delta t^2)/k^2 \\ & + 2g_2\cos[ck\Delta t]/(c^2k^4) \\ & - g_0\cos[ck\Delta t]/k^2 - g_1\sin[ck\Delta t]/(ck^3) + O(\Delta t^3) \end{aligned} \quad \text{(B13a)}$$

and for the special case of $k = 0$, we obtain

$$\begin{aligned} F(t_{n+1}) = {} & F(t_n) + dF(t_n)/dt_n \Delta t \\ & + (g_0/2 + g_1\Delta t/6 + g_2\Delta t^2/12)c^2\Delta t^2 + O(\Delta t^3). \end{aligned} \quad \text{(B13b)}$$

APPENDIX C: ENERGETIC CONSIDERATIONS FOR FINITE HILBERT SPACES

When the spatial axis is sampled by a finite number N_z of equidistant points separated by Δz, the corresponding momentum lattice covers values from $(-N_z/2+1)\ \Delta k$ to the Nyquist momentum $k_{\max} \equiv N_z\Delta k/2$ with $\Delta k = 2\pi/(N_z\Delta_z)$. If the Dirac Hamiltonian describes a free particle, this would correspond to discrete relativistic energies in the range $-[c^4 + k_{\max}^2c^2]^{1/2}$ to $-c^2$ and c^2 to $[c^4 + k_{\max}^2c^2]^{1/2}$. The question that we will address in this appendix is whether a quantum field theoretical modeling of a continuous and spatially infinitely extended system permits us to take all available discrete states in this energy range into account. The data discussed below suggest that states with energies close to the largest value on our energy grid are potentially unphysical, lead to possible violations of causality, and therefore might be omitted in order to obtain physically meaningful results.

The necessity of a required truncation (within the already finite Hilbert space) of discrete energy states to those with lower momentum is already well established for the simplest case of a free nonrelativistic particle with a Hamiltonian $h = p^2/2$. If we were to approximate the second spatial derivative by a three-point finite-difference formula, the corresponding tridiagonal Hamiltonian matrix can be diagonalized analytically and it turns out [60,61] that only the lower-lying energies have the same density $\rho(E)$ as the corresponding continuous system [which is $\rho(E) \sim E^{-1/2}$]. In fact, for larger energies, the numerical density increases with energy again,

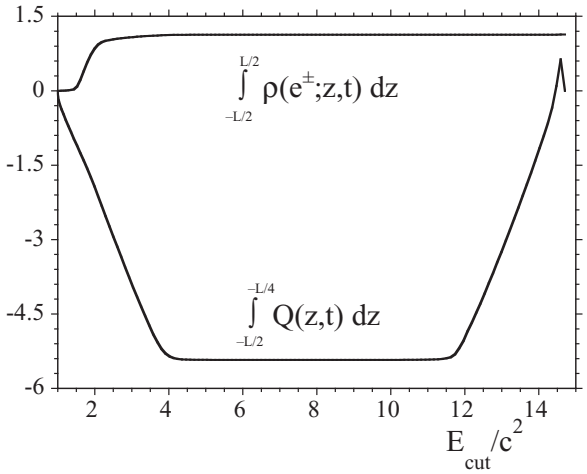

FIG. 8. The number of created particle pairs at time $t = 0.1/c$ as a function of the maximum energy E_{cut} of the discrete Hilbert space states. The second graph is the area under the polarization charge density between $z = -L/2$ and $-L/4$. (Parameters are $t = 0.05/c$, $V_0 = 3c^2$, $W = 0.5/c$, $d = 0.2$ a.u., $L = 0.4$ a.u., $N_z = 256$, $N_t = 1000$, $\kappa = 0$, $q = -1$.)

which is unphysical and requires the omission of these states for dynamical calculations.

Let us obtain a rough energy estimate for our relativistic parameters. Using the simplest case of a single supercritical barrier of height V_0 ($>2c^2$), it is known [61] that the energy range of the created particles in the (long-time) steady state is given by $c^2 < E < V_0 - c^2$. In our specific simulations above ($V_0 = 3c^2$), this corresponds to a maximum kinetic energy of c^2. If we estimate the dressing of the potential for the true energy eigenstates and include the possibility of higher energetic particles (created at times when the barrier was turned on) we might expect that states above energies $E_{\text{cut}} = 6c^2$ or $10c^2$ play dynamically no role and must be discarded in the computation of the final total polarization charge density $\rho(z,t)$.

In Fig. 8 we show the total number of created particle pairs N as a function of the energy cutoff E_{cut}. It is clear that there is no need to take higher energetic states than $E_{\text{cut}} = 5c^2$ into account. This makes sense as N is only nonzero if there is a transition from a negative to positive energy state and states with higher energy are not coupled as strongly as those close to the mass gap between $\pm c^2$.

For comparison, the second graph is the area under the total charge density between $z = -L/2$ and $-L/4$. In contrast to the number of created particles, which occur only if $V_0 > 2c^2$, this density is linearly proportional to V_0 (even for $\kappa = 0$ and $V_0 \ll 2c^2$) and is seriously affected by higher energetic states close to the unphysical maximum grid energy (here about $14.7c^2$ for $L = 0.4$ a.u. and $N_z = 256$).

In Fig. 9 we display the polarization charge density for various cutoff energies, which can be computed for $\kappa = 0$ from the time-evolved states as

$$\begin{aligned} \rho(z,t) = {} & q\Sigma_p[W_p(d;z,t)^\dagger W_p(d;z,t) \\ & - W_p(u;z,t)^\dagger W_p(u;z,t)]/2, \end{aligned} \quad \text{(C1a)}$$

$$\begin{aligned} J(z,t) = {} & qc\Sigma_p[W_p(d;z,t)^\dagger \sigma_1 W_p(d;z,t) \\ & - W_p(u;z,t)^\dagger \sigma_1 W_p(u;z,t)]/2, \end{aligned} \quad \text{(C1b)}$$

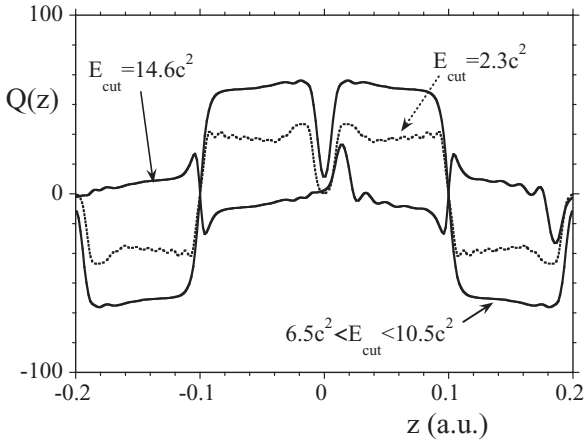

FIG. 9. The final total charge density $Q(z,t)$ at time $t = 0.1/c$ computed for various discrete Hilbert spaces, characterized by several cutoff energies E_{cut}. $E_{\text{cut}} = 2.3c^2$, $6.5c^2 < E_{\text{cut}} < 10.5c^2$ and $E_{\text{cut}} = 14.6c^2$ (Parameters are $t = 0.1/c$, $V_0 = 3c^2$, $w = 0.5/c$, $d = 0.2$ a.u., $L = 0.4$ a.u., $N_z = 256$, $N_t = 1000$, $\kappa = 0$, $q = -1$.)

where each state was evolved under the Dirac Hamiltonian $c\sigma_1 p + \sigma_3 c^2 + q V_{\text{ext}}(z)$. We used $q = -1$ in our simulations and studied an external potential [given in Eq. (4.2) with $V_{\text{ext}}(z) > 0$] that is therefore attractive for created electrons and should repel positrons to $\pm\infty$. The resulting polarization charge computed according to Eqs. (C1) with $q = -1$ is negative for $z > z_c$. As expected, the density above a cutoff of about $E_{\text{cut}} = 5c^2$ seems to be converged. In the entire range from $E_{\text{cut}} = 5c^2$ to $E_{\text{cut}} = 10c^2$ the densities are basically graphically indistinguishable, nicely suggesting that the results are converged independently of the number of included high-energy states. As a side note, we should mention that this behavior is different from the use of regulators in perturbative quantum field calculations, where the corresponding diverging integrals do depend on the particular choice of the momentum cutoff.

However, we have also included in the figure the charge density for a very high cutoff $E_{\text{cut}} = 14.6c^2$. In fact, this energy is close to the largest possible energy of our chosen grid $E_{\text{max}} = 14.7c^2$. The presence of the three spatial maxima between -0.04 a.u. $< z < 0.04$ a.u. clearly shows some unphysical noncausal behavior. The right force field (for $z > 0$) is centered at $z_c = 0.1$ a.u. with an effective extension of $W = 0.5/c$. The front edge (of the left-traveling) light cone at time $t = 0.05/c$ would be at location $z = z_c - W \pm ct$, which is $z \approx 0.05$ a.u. In other words, even if the particles created at z_c were to travel with a velocity close to $-c$, they could not have reached the region -0.04 a.u. $< z < 0.04$ a.u. where the charge density apparently has been modified from its initial value of zero.

In finishing, we should also point out that on a grid with an even number of momentum states that contains $k = 0$, the presence of the Nyquist momentum breaks the required symmetry of positive and negative momenta in our system. In other words, if all available Hilbert states were initially populated (as required in any quantum field theoretical calculation), the total current density of the vacuum would not vanish as the contribution due to the positive Nyquist momentum k_{max} cannot be cancelled out by a corresponding negative momentum as we showed at the beginning of this appendix. In the case of the total charge density, however, this asymmetry is not so crucial, as states of positive and negative energies contribute to the densities with opposite sign, while [as we have argued below Eq. (2.2)] equal momentum states with positive and negative energies move in opposite directions, such that the required cancellation of the initial current densities has to occur within each energy manifold. The latter would require an equal number of states of positive and negative momentum for each energy subspace.

[1] For a recent review, see, e.g., A. Di Piazza, C. Müller, K. Z. Hatsagortsyan, and C. H. Keitel, Rev. Mod. Phys. **84**, 1177 (2012).

[2] E. N. Nerush, I. Y. Kostyukov, A. M. Fedotov, N. B. Narozhny, N. V. Elkina, and H. Ruhl, Phys. Rev. Lett. **106**, 035001 (2011).

[3] S. S. Bulanov, V. D. Mur, N. B. Narozhny, J. Nees, and V. S. Popov, Phys. Rev. Lett. **104**, 220404 (2010).

[4] M. Ruf, G. R. Mocken, C. Müller, K. Z. Hatsagortsyan, and C. H. Keitel, Phys. Rev. Lett. **102**, 080402 (2009).

[5] R. Schützhold, H. Gies, and G. Dunne, Phys. Rev. Lett. **101**, 130404 (2008).

[6] A. R. Bell and J. G. Kirk, Phys. Rev. Lett. **101**, 200403 (2008).

[7] J. C. R. Bloch, V. A. Mizerny, A. V. Prozorkevich, C. D. Roberts, S. M. Schmidt, S. A. Smolyansky, and D. V. Vinnik, Phys. Rev. D **60**, 116011 (1999).

[8] D. V. Vinnik, A. V. Prozorkevich, S. A. Smolyanskyy, V. D. Toneev, M. B. Hecht, C. D. Roberts, and S. M. Schmidt, Eur. Phys. J. C **22**, 341 (2001).

[9] C. D. Roberts, S. M. Schmidt, and D. V. Vinnik, Phys. Rev. Lett. **89**, 153901 (2002).

[10] D. B. Blaschke, A. V. Prozorkevich, C. D. Roberts, S. M. Schmidt, and S. A. Smolyansky, Phys. Rev. Lett. **96**, 140402 (2006).

[11] D. B. Blaschke, A. V. Prozorkevich, G. Röpke, C. D. Roberts, S. M. Schmidt, D. S. Shkirmanov, and S. A. Smolyansky, Eur. Phys. J. D **55**, 341 (2009).

[12] F. Hebenstreit, J. Berges, and D. Gelfand, Phys. Rev. D **87**, 105006 (2013).

[13] F. Hebenstreit, J. Berges, and D. Gelfand, Phys. Rev. Lett. **111**, 201601 (2013).

[14] J. S. Schwinger, Phys. Rev. **82**, 664 (1951).

[15] For a review, see, e. g., W. Greiner, B. Müller, and J. Rafelski, *Quantum Electrodynamics of Strong Fields* (Springer-Verlag, Berlin, 1985).

[16] For recent experimental efforts, see, e.g., http://www.extreme-light-infrastructure.eu/

[17] R. E. Wagner, M. R. Ware, B. T. Shields, Q. Su, and R. Grobe, Phys. Rev. Lett. **106**, 023601 (2011).

[18] B. Thaller, *The Dirac Equation* (Springer, Berlin, 1992).

[19] I. Bialynicki-Birula and Z. Bialynickia-Birula, *Quantum Electrodynamics* (Pergamon, Oxford, 1975).
[20] A. D. Boozer, Eur. J. Phys. **28**, 447 (2007); Am. J. Phys. **77**, 262 (2009).
[21] J. van Bladel, IEEE Antennas Propag. Mag. **33**, 69 (1991).
[22] R. Nevels and C.-S. Shin, IEEE Antennas Propag. Mag. **43**, 70 (2001).
[23] J. A. Fleck, J. R. Morris, and M. D. Feit, Appl. Phys. **10**, 129 (1976).
[24] A. D. Bandrauk and H. Shen, J. Phys. A **27**, 7147 (1994).
[25] J. W. Braun, Q. Su, and R. Grobe, Phys. Rev. A **59**, 604 (1999).
[26] G. R. Mocken and C. H. Keitel, Comput. Phys. Commun. **178**, 868 (2008).
[27] M. Ruf, H. Bauke, and C. H. Keitel, J. Comput. Phys. **228**, 9092 (2009).
[28] M. Wakano, Prog. T. Phys. **35**, 1117 (1966).
[29] V. Delgado, Proc. Math. Soc. **69**, 289 (1978).
[30] R. T. Glassey and W. A. Strauss, J. Math. Phys. **20**, 454 (1979).
[31] A. Das, J. Math. Phys. **34**, 3986 (1993).
[32] A. G. Lisi, J. Phys. A **28**, 5385 (1995).
[33] M. J. Esteban, V. Georgiev, and E. Sere, Calc. Var. **4**, 265 (1996).
[34] H. S. Booth and C. J. Radford, J. Math. Phys. **38**, 1257 (1997).
[35] V. Benci and D. Fortunato, Topol. Meth. Nonl. Anal. **11**, 283 (1998).
[36] C. Radford, Proc. Inst. Math. Ukraine **43**, 666 (2002).
[37] W. Bao and X.-G. Li, J. Comput. Phys. **199**, 663 (2004).
[38] Z. Huang, J. Shi, P. A. Markowich, C. Sparber, and C. Zheng, J. Comput. Phys. **208**, 761 (2005).
[39] E. Lorin, S. Chelkowski, and A. Bandrauk, Comput. Phys. Comm. **177**, 908 (2007).
[40] P. Krekora, Q. Su, and R. Grobe, Phys. Rev. A **70**, 054101 (2004).
[41] For a review, see, e.g., T. Cheng, Q. Su, and R. Grobe, Contemp. Phys. **51**, 315 (2010).
[42] F. Sauter, Z. Phys. **69**, 742 (1931).
[43] P. Krekora, Q. Su, and R. Grobe, Phys. Rev. Lett. **93**, 043004 (2004).
[44] P. Krekora, Q. Su, and R. Grobe, Phys. Rev. A **73**, 022114 (2006).
[45] C. C. Gerry, Q. Su, and R. Grobe, Phys. Rev. A **74**, 044103 (2006).
[46] B. R. Holstein, Am. J. Phys. **66**, 507 (1998).
[47] B. R. Holstein, Am. J. Phys. **67**, 499 (1999).
[48] P. Krekora, Q. Su, and R. Grobe, Phys. Rev. Lett. **92**, 040406 (2004).
[49] R. E. Wagner, P. J. Peverly, Q. Su, and R. Grobe, Laser Phys. **11**, 221 (2001).
[50] N. I. Chott, Q. Su, and R. Grobe, Phys. Rev. A **76**, 010101-1(R) (2007).
[51] T. Cheng, E. R. Gospodarczyk, Q. Su, and R. Grobe, Ann. Phys. **325**, 265 (2010).
[52] B. Müller, H. Peitz, J. Rafelski, and W. Greiner, Phys. Rev. Lett. **28**, 1235 (1972).
[53] P. Krekora, K. Cooley, Q. Su, and R. Grobe, Laser Phys. **15**, 282 (2005).
[54] S. S. Schweber, *An Introduction to Relativistic Quantum Field Theory* (Harper & Row, New York, 1962).
[55] M. E. Peskin and D. V. Schroeder, *An Introduction to Quantum Field Theory* (Westview, Boulder, 1995).
[56] M. Srednicki, *Quantum Field Theory* (Cambridge University Press, Cambridge, England, 2007).
[57] E. V. Stefanovich, *Relativistic Quantum Dynamics: A Non-traditional Perspective on Space, Time, Particles, Fields, and Action-at-a-distance* (Mountain View, 2004), available at arXiv:physics/0504062v13 [physics.gen-ph].
[58] I. Bialynicki-Birula, in *Proceedings of the NATO Advanced Study Institute on Quantum Electrodynamics and Quantum Optics*, edited by A. O. Barut (Plenum, New York, 1984), p. 41.
[59] For exceptions, see e.g., A. Taflove and S. C. Hagness, *Computational Electrodynamics: The Finite-Difference Time-Domain Method*, 3rd ed. (Artech House, Norwood, 2005).
[60] For example, see M. Ruf, C. Müller, and R. Grobe, J. Phys. A **44**, 345205 (2011).
[61] O. Klein, Z. Phys. **53**, 157 (1929); **41**, 407 (1927). For thorough discussions, see also Chaps. 5 and 10.7 in Ref. [15], or Refs. [46–48].